DOI: 10.1002/ejic.200600273

Amine-Intercalated Layered Sn^{II} Phosphates with Open-Framework Structures

Padmini Ramaswamy[a] and Srinivasan Natarajan*[a]

Keywords: Template synthesis / X-ray diffraction / Layered compounds / Hydrogen bonds / Tin / Phosphorus

Three new Sn^{II} phosphate materials, $[NH_3(CH_2)_3NH_2(CH_2)_2NH_2(CH_2)_3NH_3]\cdot 2[Sn_2P_2O_8]$ (**I**), $[(N_2C_5H_{14})_2][Sn_4P_4O_{16}]\cdot 3H_2O$ (**II**) and $[(N_2C_5H_{14})][Sn_2P_2O_8]\cdot H_2O$ (**III**), have been synthesised by means of hydrothermal methods using *N*,*N*′-bis(3-aminopropyl)ethylenediamine (BAPEN; for **I**) and homopiperazine (H-PIP; for **II** and **III**), respectively, as the structure-directing organic amines. The solids **I**–**III** have layered architectures. The structures of all three compounds consist of strictly alternating vertex-sharing trigonal-pyramidal SnO_3 and tetrahedral PO_4 moieties forming infinite layers possessing apertures bound by 4- and 8-T atoms (T = Sn, P). The distorted 4- and 8-membered apertures within the layers suggest the subtle influence of the lone-pair of electrons of Sn^{II} on the structure. The interlamellar space is occupied by the protonated organic amine molecules which interact with the framework through N–H···O hydrogen bonding. The compounds **I**–**III** bear some structural relationship to the layered zinc phosphite phases.

Introduction

The wide structural diversity along with the potential applications in the areas of catalysis, sorption and separation processes are the reasons for the continued interest in the area of open-framework materials.[1] The continuing research has clearly established that new materials with novel structures can be made in the presence of structure-directing organic amines.[2] It is now firmly established that tin(II) phosphates exhibiting open-framework structures can be prepared employing hydrothermal methods.[3–13] The chemistry of divalent tin and its related compounds, especially the phosphates[3–13] and the phosphonates,[14–16] continues to yield unexpected results with the lone-pair associated with Sn^{II} playing a significant role. In the family of tin phosphates, the isolation of solids having zero-,[3] one-,[4,5] two-[6–8] and three-dimensionally[9–13] extended networks clearly indicates that the system is versatile like the other family of open-framework phosphates. It is noteworthy that one of the basic structural building blocks, present in most of the phosphate based open-framework solids, is a four-membered ring made of $[M_2P_2O_4]$ units. The analogue with M = Sn has also been isolated and characterised.[3] The main structural features present in all the tin phosphate and phosphonate materials are the presence of either three- and/or four-coordinated Sn^{II} atoms that are vertex-linked to PO_4 tetrahedra forming channels and cavities. In general, it is observed that the Sn/P ratio in many of the tin phosphates is >1. In this paper, we report the hydrothermal synthesis and structures of three simple open-framework tin(II) phosphates, $[NH_3(CH_2)_3NH_2(CH_2)_2NH_2(CH_2)_3NH_3]\cdot 2[Sn_2P_2O_8]$ (**I**), $[(N_2C_5H_{14})_2][Sn_4P_4O_{16}]\cdot 3H_2O$ (**II**) and $[(N_2C_5H_{14})][Sn_2P_2O_8]\cdot H_2O$ (**III**), having an Sn/P ratio of 1.0. The compounds were prepared in the presence of *N*,*N*′-bis(3-aminopropyl)ethylenediamine (BAPEN; for **I**) and homopiperazine (H-PIP; for **II** and **III**), respectively, as the structure-directing agent.

Results and Discussion

Three new Sn^{II} phosphates, $[\{NH_3(CH_2)_3NH_2(CH_2)_2NH_2(CH_2)_3NH_3\}_2]\cdot 2[Sn_2P_2O_8]$ (**I**), $[(N_2C_5H_{14})_2][Sn_4P_4O_{16}]\cdot 3H_2O$ (**II**) and $[(N_2C_5H_{14})][Sn_2P_2O_8]\cdot H_2O$ (**III**), were synthesised using hydrothermal methods. As a result of the synthesis being kinetically controlled solvent-mediated reactions, there is no relationship between the starting synthesis mixture composition and the stoichiometry of the final solid product. The compounds **I**–**III** have similar structures consisting of layers that are intercalated by the structure-directing organic amine molecules. The structures are based on a network of strictly alternating SnO_3 and PO_4 units. These units form infinite layers with the incorporation of the organic amine in the fully protonated form.

The asymmetric unit of **I** contains 18 independent non-hydrogen atoms, of which two Sn and P atoms are crystallographically independent. The structure of **I** is constructed from a network of SnO_3 and PO_4 units forming infinite layers which are anionic. The connectivity between these moieties creates 4- and 8-membered rings along the *b*-axis. The polyhedral connectivity between the SnO_3 and PO_4 units forming the two-dimensional layer is shown in Fig-

[a] Framework Solids Laboratory, Solid State and Structural Chemistry Unit, Indian Institute of Science
Bangalore 560012, India
E-Mail: snatarajan@sscu.iisc.ernet.in
Supporting information for this article is available on the WWW under http://www.eurjic.org or from the author.

ure 1. As can be noted, each four-membered ring within the layer is connected to four eight-membered rings and each eight-membered ring is attached to four four-membered rings. The organic amine molecules (BAPEN) balance the charges of the anionic layers and are located in the spaces between the layers. The individual layers are held together by the fully protonated BAPEN molecules through hydrogen bonding interactions (Figures 2a and b).

The asymmetric unit of **II** contains 42 independent non-hydrogen atoms, of which 24 atoms belong to the framework and the remaining atoms to the lattice water and amine guest molecules. There are four Sn and P atoms that

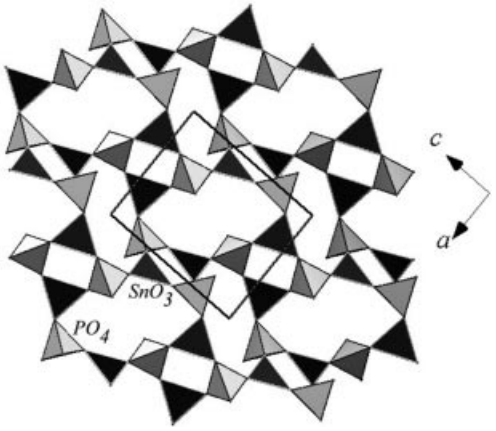

Figure 1. Polyhedral view of a single layer in $[NH_3(CH_2)_3NH_2(CH_2)_2NH_2(CH_2)_3NH_3]\cdot 2[Sn_2P_2O_8]$ (**I**) in the *ac* plane.

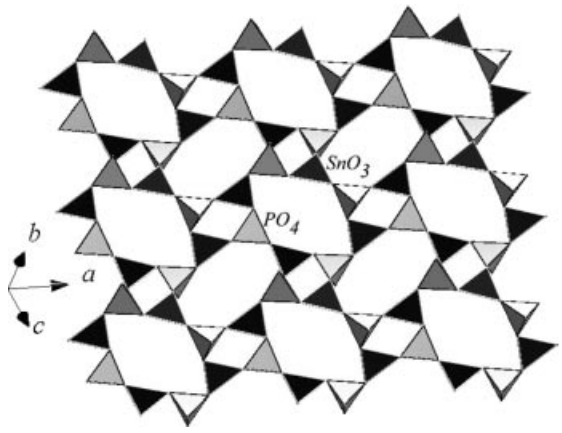

Figure 3. Polyhedral view of a single layer in $[(N_2C_5H_{14})_2][Sn_4P_4O_{16}]\cdot 3H_2O$ (**II**).

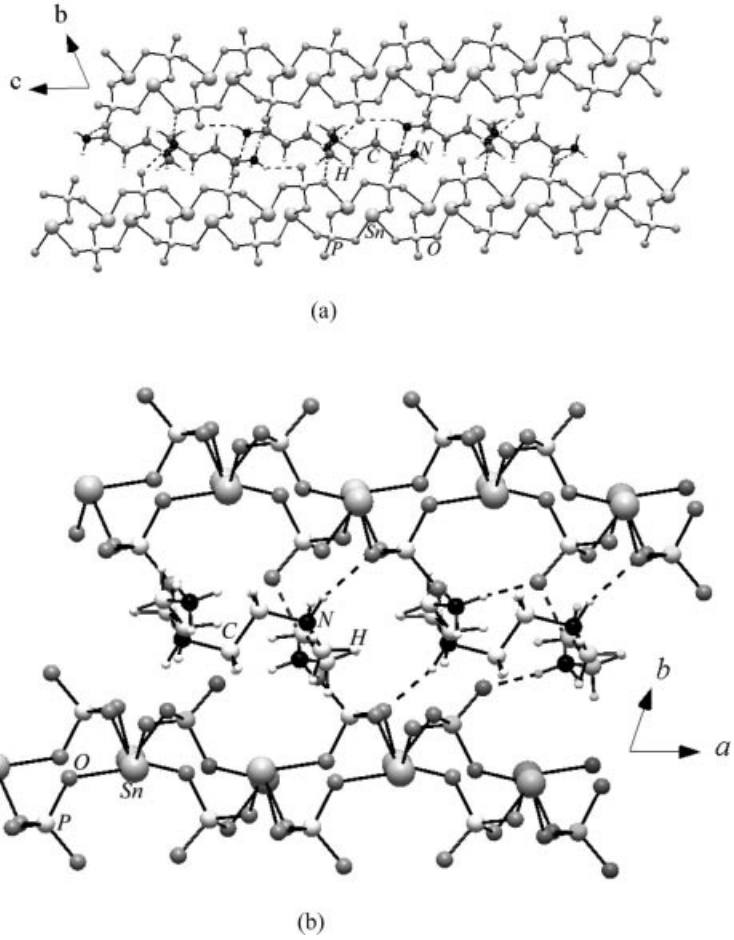

Figure 2. (a) Arrangement of the layers in **I** in the *bc* plane. (b) Arrangement of the layers in **I** in the *ab* plane. The dotted lines in both the cases represent possible hydrogen-bonding interactions.

are crystallographically independent. Similar to **I**, the structure of **II** is constructed by a network of SnO_3 and PO_4 units forming infinite layers that are anionic. The connectivity between these moieties creates 4- and 8-membered rings in the *ab* plane (Figure 3). In **II**, there appear to be two types of 4- and 8-membered apertures, the arrangement of which gives a three-dimensional character to the layers. The differences in the sizes and shapes of the apertures may be attributed to the relative positioning of the lone-pair of electrons on Sn^{II}. The charge-compensating protonated organic amine cations (H-PIP) are located in the inter-lamellar regions and are involved in hydrogen bonding through N–H···O, C–H···O and O–H···O interactions (Figure 4).

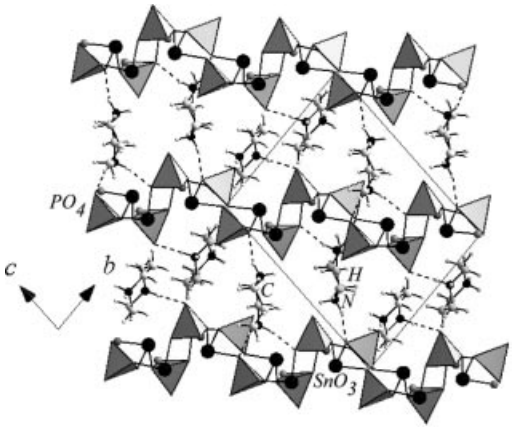

Figure 4. Arrangement of the layers in **II** in the *bc* plane. Dotted lines represent possible hydrogen-bonding interactions. The lattice water molecules are not shown.

The asymmetric unit of **III** contains 20 independent non-hydrogen atoms, of which two Sn and P atoms are crystallographically independent. The connectivity between the SnO_3 and PO_4 units creates 4- and 8-membered rings within the layer in the *bc* plane. The polyhedral connectivity of a single layer is shown in Figure 5. As can be noted, each 4-membered ring within the layer is connected to four 8-membered rings and each 8-membered ring is attached to four 4-membered rings. The 8-membered rings are considerably more distorted compared with those in the structures of **I** and **II**. The organic amine molecules (H-PIP) balance the charges of the anionic layers and are located in the spaces between the layers. The individual layers are held together by the protonated H-PIP molecules through hydrogen-bonding interactions (Figure 6).

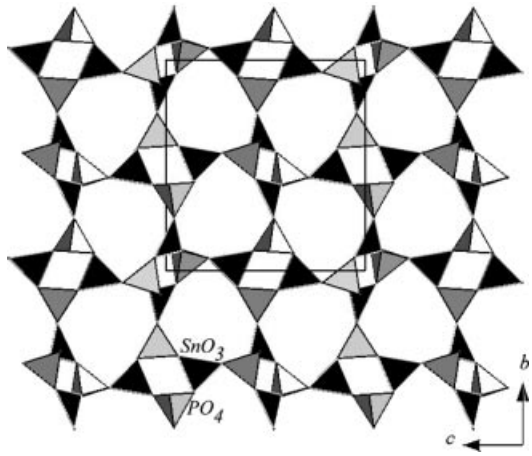

Figure 5. Polyhedral view of a single layer in $[(N_2C_5H_{14})][Sn_2P_2O_8]\cdot H_2O$ (**III**) in the *bc* plane.

Compounds **I**–**III** therefore represent examples of open-framework solids possessing alternating anionic and cationic layers. It may be noted that one of the basic building units present in many of the tin phosphates and other related materials, namely $M_2P_2O_4$ units (M = Sn in the present case),[3] can be observed in all the structures.

The Sn–O bond lengths are in the range from 2.0635(18) to 2.1234(17) Å and the O–Sn–O bond angles are between 82.76(6) and 93.42(14)° which is typical of three-coordinate Sn^{II} centres[3–13] (Tables 1, 2 and 3). The Sn atoms are linked to P by means of the oxygen links. The P atoms are

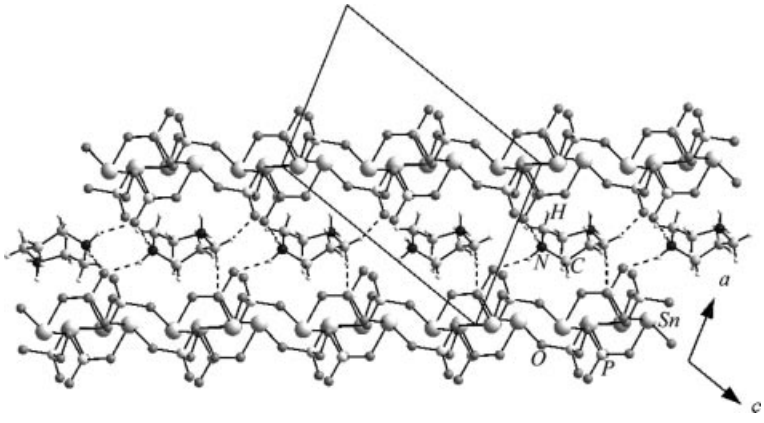

Figure 6. Arrangement of layers in **III** in the *ac* plane. Dotted lines represent possible hydrogen-bonding interactions. The lattice water molecules are not shown.

Table 1. Selected bond lengths [Å] and bond angles [°] for $[NH_3(CH_2)_3NH_2(CH_2)_2NH_2(CH_2)_3NH_3]\cdot 2[Sn_2P_2O_8]$ (**I**).

Sn(1)–O(1)	2.0911(17)	P(1)–O(5)[a]	1.5412(17)
Sn(1)–O(2)	2.0899(18)	P(1)–O(6)[b]	1.5475(17)
Sn(1)–O(3)	2.1035(16)	P(1)–O(3)	1.5510(16)
Sn(2)–O(4)	2.0635(18)	P(2)–O(8)	1.4928(18)
Sn(2)–O(5)	2.0957(18)	P(2)–O(4)	1.5268(17)
Sn(2)–O(6)	2.1234(17)	P(2)–O(1)	1.5442(18)
P(1)–O(7)	1.5022(18)	P(2)–O(2)[c]	1.5448(19)
O(2)–Sn(1)–O(1)	89.12(8)	O(8)–P(2)–O(4)	111.89(12)
O(2)–Sn(1)–O(3)	86.52(7)	O(8)–P(2)–O(1)	109.78(11)
O(1)–Sn(1)–O(3)	82.76(6)	O(4)–P(2)–O(1)	107.85(11)
O(4)–Sn(2)–O(5)	84.62(7)	O(8)–P(2)–O(2)[c]	112.26(13)
O(4)–Sn(2)–O(6)	88.67(7)	O(4)–P(2)–O(2)[c]	107.20(11)
O(5)–Sn(2)–O(6)	88.13(7)	O(1)–P(2)–O(2)[c]	107.65(11)
O(7)–P(1)–O(5)[a]	108.40(11)	P(2)–O(1)–Sn(1)	119.79(10)
O(7)–P(1)–O(6)[b]	112.81(11)	P(2)[c]–O(2)–Sn(1)	122.75(11)
O(5)[a]–P(1)–O(6)[b]	108.79(10)	P(1)–O(3)–Sn(1)	122.80(9)
O(7)–P(1)–O(3)	110.93(10)	P(2)–O(4)–Sn(2)	130.82(11)
O(5)[a]–P(1)–O(3)	109.29(10)	P(1)[d]–O(5)–Sn(2)	126.37(11)
O(6)[b]–P(1)–O(3)	106.55(9)	P(1)[b]–O(6)–Sn(2)	120.31(10)

Symmetry transformations used to generate equivalent atoms: [a] $x, y, z + 1$. [b] $-x, -y, -z$. [c] $-x + 1, -y, -z$. [d] $x, y, z - 1$.

Table 2. Selected bond lengths [Å] and bond angles [°] for $[(N_2C_5H_{14})_2][Sn_4P_4O_{16}]\cdot 3H_2O$ (**II**).

Sn(1)–O(1)	2.082(4)	P(1)–O(4)	1.545(4)
Sn(1)–O(2)	2.092(4)	P(1)–O(6)	1.558(4)
Sn(1)–O(3)	2.124(4)	P(2)–O(14)	1.510(4)
Sn(2)–O(4)[a]	2.079(4)	P(2)–O(5)	1.535(4)
Sn(2)–O(5)[b]	2.101(4)	P(2)–O(11)	1.546(4)
Sn(2)–O(6)	2.112(4)	P(2)–O(2)	1.547(4)
Sn(3)–O(7)	2.095(4)	P(3)–O(15)	1.517(4)
Sn(3)–O(8)	2.107(4)	P(3)–O(10)[c]	1.532(4)
Sn(3)–O(9)	2.115(3)	P(3)–O(7)	1.540(4)
Sn(4)–O(10)	2.082(4)	P(3)–O(9)[d]	1.551(4)
Sn(4)–O(11)	2.099(4)	P(4)–O(16)	1.500(4)
Sn(4)–O(12)	2.115(4)	P(4)–O(8)	1.533(4)
P(1)–O(13)	1.499(4)	P(4)–O(3)	1.554(4)
P(1)–O(1)	1.535(4)	P(4)–O(12)	1.557(4)
O(1)–Sn(1)–O(2)	85.96(15)	O(15)–P(3)–O(10)[c]	109.4(2)
O(1)–Sn(1)–O(3)	90.65(15)	O(15)–P(3)–O(7)	110.6(2)
O(2)–Sn(1)–O(3)	92.12(15)	O(10)[c]–P(3)–O(7)	108.2(2)
O(4)[a]–Sn(2)–O(5)[b]	89.10(15)	O(15)–P(3)–O(9)[d]	110.6(2)
O(4)[a]–Sn(2)–O(6)	88.93(15)	O(10)[c]–P(3)–O(9)[d]	109.3(2)
O(5)[b]–Sn(2)–O(6)	85.25(14)	O(7)–P(3)–O(9)[d]	108.6(2)
O(7)–Sn(3)–O(8)	89.12(15)	O(16)–P(4)–O(8)	110.8(2)
O(7)–Sn(3)–O(9)	88.60(14)	O(16)–P(4)–O(3)	110.2(2)
O(8)–Sn(3)–O(9)	87.21(14)	O(8)–P(4)–O(3)	109.5(2)
O(10)–Sn(4)–O(11)	85.27(14)	O(16)–P(4)–O(12)	111.7(2)
O(10)–Sn(4)–O(12)	86.81(14)	O(8)–P(4)–O(12)	108.4(2)
O(11)–Sn(4)–O(12)	93.42(14)	O(3)–P(4)–O(12)	106.1(2)
O(13)–P(1)–O(1)	111.9(2)	P(1)–O(1)–Sn(1)	129.0(2)
O(13)–P(1)–O(4)	112.3(2)	P(2)–O(2)–Sn(1)	123.0(2)
O(1)–P(1)–O(4)	107.7(2)	P(4)–O(3)–Sn(1)	119.1(2)
O(13)–P(1)–O(6)	109.4(2)	P(1)–O(4)–Sn(2)[a]	127.4(2)
O(1)–P(1)–O(6)	106.6(2)	P(2)–O(5)–Sn(2)[b]	126.5(2)
O(4)–P(1)–O(6)	108.7(2)	P(1)–O(6)–Sn(2)	121.2(2)
O(14)–P(2)–O(5)	111.4(2)	P(3)–O(7)–Sn(3)	122.2(2)
O(14)–P(2)–O(11)	109.5(2)	P(4)–O(8)–Sn(3)	131.4(2)
O(5)–P(2)–O(11)	109.3(2)	P(3)[d]–O(9)–Sn(3)	123.2(2)
O(14)–P(2)–O(2)	110.9(2)	P(3)[c]–O(10)–Sn(4)	129.3(2)
O(5)–P(2)–O(2)	107.8(2)	P(2)–O(11)–Sn(4)	123.8(2)
O(11)–P(2)–O(2)	107.9(2)	P(4)–O(12)–Sn(4)	121.6(2)

Symmetry transformations used to generate equivalent atoms: [a] $-x + 1, -y + 1, -z + 1$. [b] $-x, -y + 1, -z + 1$. [c] $-x, -y, -z + 2$. [d] $-x + 1, -y, -z + 2$.

tetrahedrally linked to oxygen atoms with P–O distances in the range of 1.493(2) to 1.558(4) Å and O–P–O bond angles in the range of 106.1(2) to 112.8(2)°. The P(1)–O(7) and P(2)–O(8) bonds with distances of 1.5022(18) and 1.4928(18) Å for **I**, P(1)–O(13), P(2)–O(14), P(3)–O(15) and P(4)–O(16) bonds with distances of 1.499(4), 1.510(4), 1.517(4) and 1.500(4) Å for **II** and P(1)–O(7) and P(2)–O(8) bonds with distances of 1.506(3) and 1.510(3) Å for **III** are all formally P=O double bonds. Terminal P=O groups in, for example $H_3PO_4\cdot 0.5H_2O$, are 1.485 and 1.495 Å in length.[17] The various bond lengths and angles observed in compounds **I**–**III** are in good agreement with other tin phosphate open-framework structures.[3–13] Selected bond lengths and angles are listed in Tables 1, 2 and 3 for **I**, **II** and **III**, respectively.

Table 3. Selected bond lengths [Å] and bond angles [°] for $[N_2C_5H_{14}][Sn_2P_2O_8]\cdot H_2O$ (**III**).

Sn(1)–O(1)	2.075(3)	P(1)–O(4)[a]	1.546(3)
Sn(1)–O(2)	2.086(3)	P(1)–O(6)[b]	1.547(3)
Sn(1)–O(3)	2.100(3)	P(1)–O(1)	1.548(3)
Sn(2)–O(4)	2.081(3)	P(2)–O(8)	1.510(3)
Sn(2)–O(5)	2.114(3)	P(2)–O(5)	1.546(3)
Sn(2)–O(6)	2.114(3)	P(2)–O(2)[c]	1.546(3)
P(1)–O(7)	1.506(3)	P(2)–O(3)	1.550(3)
O(1)–Sn(1)–O(2)	87.32(11)	O(8)–P(2)–O(5)	111.61(16)
O(1)–Sn(1)–O(3)	85.90(11)	O(8)–P(2)–O(2)[c]	109.41(16)
O(2)–Sn(1)–O(3)	90.42(11)	O(5)–P(2)–O(2)[c]	108.12(16)
O(4)–Sn(2)–O(5)	84.35(11)	O(8)–P(2)–O(3)	112.58(16)
O(4)–Sn(2)–O(6)	88.91(12)	O(5)–P(2)–O(3)	106.81(15)
O(5)–Sn(2)–O(6)	86.08(11)	O(2)[c]–P(2)–O(3)	108.15(16)
O(7)–P(1)–O(4)[a]	110.40(16)	P(1)–O(1)–Sn(1)	129.44(17)
O(7)–P(1)–O(6)[b]	112.59(16)	P(2)[c]–O(2)–Sn(1)	124.39(16)
O(4)[a]–P(1)–O(6)[b]	108.16(16)	P(2)–O(3)–Sn(1)	123.33(15)
O(7)–P(1)–O(1)	110.33(16)	P(1)[d]–O(4)–Sn(2)	125.01(17)
O(4)[a]–P(1)–O(1)	108.82(17)	P(2)–O(5)–Sn(2)	123.74(15)
O(6)[b]–P(1)–O(1)	106.39(16)	P(1)[e]–O(6)–Sn(2)	123.96(16)

Symmetry transformations used to generate equivalent atoms: [a] $-x + ½, y + ½, -z + ½$. [b] $x + ½, -y + ½, z + ½$. [c] $-x, -y + 1, -z$. [d] $-x + ½, y - ½, -z + ½$. [e] $x - ½, -y + ½, z - ½$.

The proton-decoupled ^{31}P pulsed MAS NMR spectra of **I** and **III**, shown in Figures 7a and b, clearly indicate the presence of two phosphorus sites with chemical shifts of δ_{iso} = 2.58 and 0.116 ppm for **I** and δ_{iso} = –3.475 and –4.507 ppm for **III**. The differences in the chemical shifts may be attributed to the involvement of the phosphate tetrahedra in hydrogen-bonding interactions. The observation of two distinct chemical shift peaks in the MAS NMR spectra indicates the presence of two crystallographically independent P sites which is in agreement with the single-crystal X-ray crystallographic data. Similar chemical shift values have been observed in other phosphate compounds.[18]

The lone pair of electrons on Sn^{II} appears to play an important role in the present structures. The stereoactive lone-pair of electrons manifests itself in the lattice by creating open spaces between the two layers in the tin phosphates. It is likely that the differences in the arrangement of the 4- and 8-membered apertures within the layers, observed in the present compounds, are also subtly influenced by the presence of the lone-pair electrons. The lone-pair of

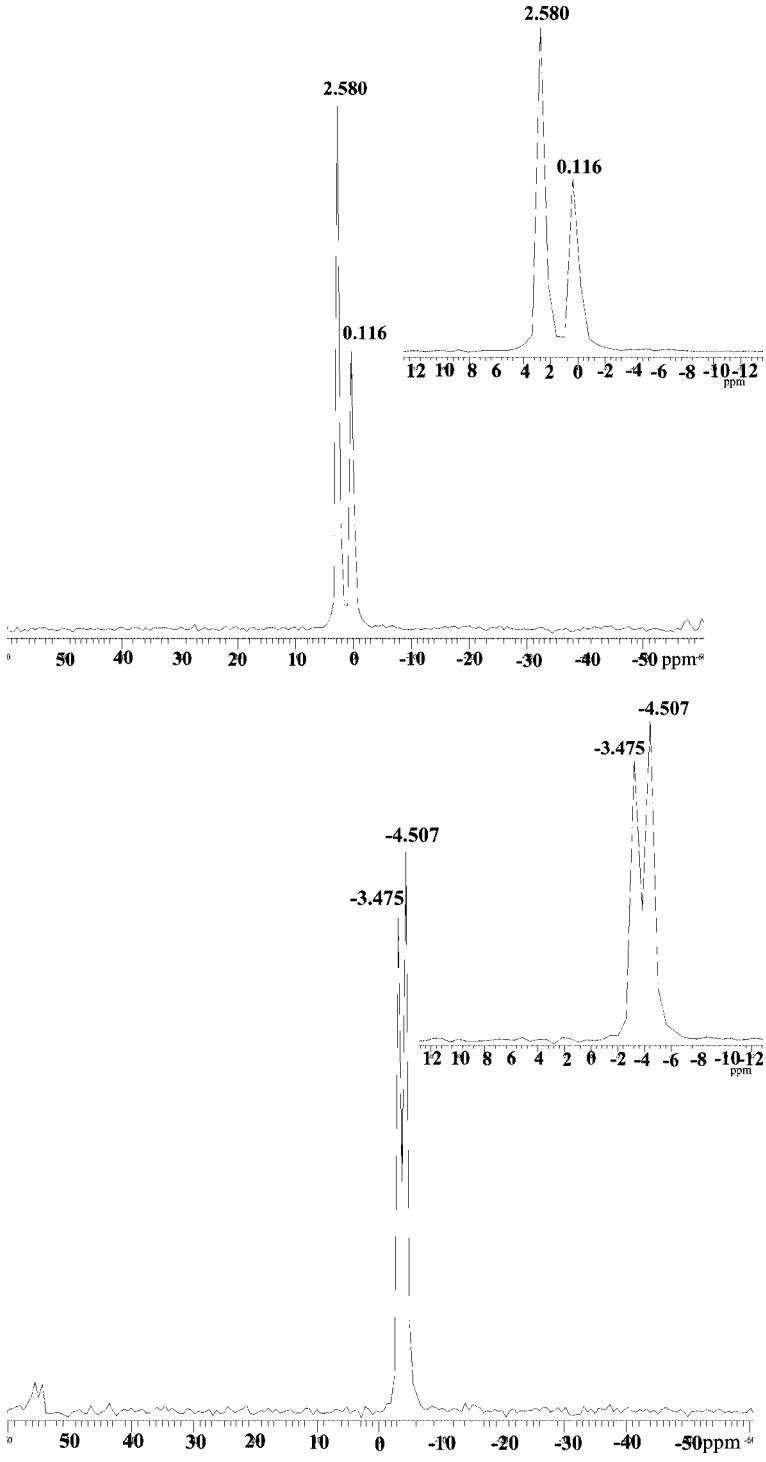

Figure 7. ^{31}P-CPMAS NMR spectra for (a) $[NH_3(CH_2)_3NH_2(CH_2)_2NH_2(CH_2)_3NH_3]\cdot 2[Sn_2P_2O_8]$ (**I**) and (b) $[(N_2C_5H_{14})][Sn_2P_2O_8]\cdot H_2O$ (**III**).

electrons on Sn^{II} generally points in a direction perpendicular to the plane of the layers. This is also expected since the amine molecules are cationic and located between the layers which would facilitate favourable interactions with the lone-pair of electrons. Similar lone-pair electron positions have been observed in many other layered Sn^{II} phosphate materials.[6–8]

Multipoint hydrogen-bonding interactions help maintain structural stability and possibly help in the formation of many of the open-framework materials that have low-dimensional character.[3–8,19–24] In the present structures **I**–**III**, the hydrogen atoms of the amine molecule interact strongly with the framework oxygen atoms, especially with the double-bonded ones. Thus, a large number of N–H···O

and C–H···O hydrogen-bonding interactions has been observed in **I**–**III**. In addition, the lattice water molecules also participate in hydrogen-bonding O–H···O interactions. Selected hydrogen-bonding interactions, observed in **I**–**III**, are listed in Table 4. The present compounds **I**–**III** thus provide good examples of multipoint hydrogen bonding and illustrate the importance of them in the structural stability of two-dimensional solids.

Table 4. Selected hydrogen-bonding interactions in $[NH_3(CH_2)_3NH_2(CH_2)_2NH_2(CH_2)_3NH_3]\cdot 2[Sn_2P_2O_8]$ (**I**), $[(N_2C_5H_{14})_2][Sn_4P_4O_{16}]\cdot 3H_2O$ (**II**) and $[(N_2C_5H_{14})][Sn_2P_2O_8]\cdot H_2O$ (**III**).

Moiety	D–H	A–H	D–A	D–H···A
I				
N(1)–H(1)···O(5)[a]	0.89	2.40	3.215(3)	152
N(1)–H(2)···O(8)[a]	0.89	1.90	2.765(3)	162
N(1)–H(3)···O(8)[b]	0.89	1.87	2.717(3)	158
N(2)–H(10)···O(7)[c]	0.90	1.78	2.665(3)	166
N(2)–H(11)···O(3)[d]	0.90	1.95	2.828(3)	163
II				
N(1)–H(1)···O(100)	0.90	1.83	2.664(8)	154
N(1)–H(2)···O(14)[d]	0.90	1.99	2.774(7)	175
N(2)–H(9)···O(200)	0.90	1.79	2.687(8)	175
N(2)–H(10)···O(15)[d]	0.90	1.78	2.672(7)	170
N(3)–H(15)···O(300)[b]	0.90	1.85	2.728(8)	165
N(3)–H(16)···O(9)[b]	0.90	2.05	2.891(7)	155
N(4)–H(23)···O(3)	0.90	1.95	2.828(7)	166
N(4)–H(24)···O(6)	0.90	1.94	2.789(7)	158
O(100)–H(101)···O(14)[b]	0.86	1.91	2.668(7)	148
O(100)–H(102)···O(15)[e]	0.86	1.81	2.634(7)	161
O(200)–H(201)···O(13)[a]	0.86	1.80	2.630(7)	165
O(200)–H(202)···O(16)[b]	0.85	1.96	2.760(9)	157
C(5)–H(13)···O(7)	0.97	2.39	3.198(8)	141
C(7)–H(20)···O(13)[b]	0.97	2.52	3.442(9)	159
C(8)–H(22)···O(2)[b]	0.97	2.53	3.446(8)	158
C(10)–H(27)···O(100)	0.97	2.58	3.424(15)	145
C(10)–H(28)···O(16)	0.97	2.47	3.438(16)	174
III				
N(1)–H(1)···O(8)[a]	0.90	1.94	2.773(5)	153
N(1)–H(2)···O(8)[c]	0.90	1.85	2.744(5)	175
C(2)–H(5)···O(2)[c]	0.97	2.45	3.364(5)	157
C(2)–H(6)···O(7)[b]	0.97	2.39	3.348(5)	172
C(3)–H(4)···O(5)	0.97	1.98	2.918(4)	161
C(3)–H(8)···O(7)[c]	0.97	1.73	2.664(5)	160

Symmetry transformations used to generate equivalent atoms: **I**: [a] $-x, 1-y, 1-z$. [b] $1-x, 1-y, -z$. [c] $x, y, 1+z$. [d] $-x, 1-y, -z$. **II**: [a] $1-x, 1-y, 1-z$. [b] $-x, 1-y, 1-z$. [c] $1-x, -y, 1-z$. [d] $1+x, y, -1+z$. [e] $x, y, -1+z$. **III**: [a] $½+x, ½-y, -½+z$. [b] $½+x, ½-y, ½+z$. [c] $-x, ½+y, ½-z$.

Structurally, the present compounds possess many features that are similar to other previously known open-framework solids, especially in Sn^{II} phosphates with two-dimensional structures.[6–8] The layered arrangements in **II** and **III**, however, appear to be unique. Additionally, the Sn^{II} phosphates can be compared with the structures of the recently discovered layered zinc phosphite networks.[23,24] While the Sn^{II} phosphate structures are built up from SnO_3 trigonal pyramids and PO_4 tetrahedra, the ZnO_4 tetrahedra and PO_3 pseudo-tetrahedral units are vertex-linked in the zinc phosphite structures. Thus, the net available vertices for bonding in both the cases are similar. In the zinc phosphites, the fourth vertex of the pseudo-tetrahedra is occupied by a P–H bond and in the Sn^{II} phosphates the fourth vertex is occupied by the lone-pair of electrons of the Sn^{II} ions. Illustrative examples of some of the previously reported zinc phosphite structures in which the layers have 4- and 8-membered apertures along with the layer arrangement of **I** and **II** are shown in Figure 8. In the zinc phosphites, $[C_2N_2H_{10}][Zn_2(HPO_3)_3]$[23] and $[(C_4N_2H_{12})(C_5NH_4)]_4[Zn_6(HPO_3)_8]$,[24] (Figures 8a and b), the 8-membered rings are connected edge-wise and are separated by edge-sharing 4-membered rings. In the zinc phosphite $[C_3NH_{10}]_2[Zn_3(HPO_3)_4]$,[24] the connectivity within the layers is identical to that found in **I** (Figures 8c and d) which clearly establishes the net available vertices for bonding in both the structures. The structural features observed in the structures of **II** and **III** (Figures 8e and f) appear to be unique and, to the best of our knowledge, there are no corresponding zinc phosphite structures known in the literature. It may be noted that the 8-membered rings in **III** are distorted compared with those in **I** and **II**, indicating the subtle control exhibited, on the structure of **III**, by the lone-pair of electrons on Sn^{II}. In general, the layered phosphate/phosphite structures are held together by strong hydrogen-bonding interactions involving the P=O groups and the organic amine template molecules. The presence of trigonal-pyramidal SnO_3 and tetrahedral PO_4 units linking to form the layers and the interactions with the organic amine molecule renders the unique architectures seen in these materials.

Conclusions

The synthesis of three new layered tin(ii) phosphate materials, $[NH_3(CH_2)_3NH_2(CH_2)_2NH_2(CH_2)_3NH_3]\cdot 2[Sn_2P_2O_8]$ (**I**), $[(N_2C_5H_{14})_2][Sn_4P_4O_{16}]\cdot 3H_2O$ (**II**) and $[(N_2C_5H_{14})][Sn_2P_2O_8]\cdot H_2O$ (**III**), consisting of alternating inorganic and organic layers has been accomplished. These materials, together with the previously reported Sn^{II} phosphate and phosphonate solids, illustrate the profound structural influences of relatively minor modifications in the reaction conditions and/or changes in the starting source of tin. The present solids represent another example illustrating the importance of multipoint hydrogen bonding in the synthesis and stability of lower dimensional open-framework materials. The structures appear to a have close similarity to the phosphite-based ones. The stereoactive lone-pair of electrons on Sn^{II} appears to subtly control the formation of the structure by manifesting itself in the open spaces. Our continuing research on the Sn^{II} phosphates indicates that other related structures are formed under hydrothermal conditions in the presence of other structure-directing agents. While the isolation of a two-dimensional solid with strictly alternating SnO_3 and PO_4 moieties provides information about the stereochemical consequences of the Sn^{II} lone-pair of electrons, further evaluation is required to exploit the structure-directing influences of this unit in the presence of other organic amines in the synthesis of open-framework materials.

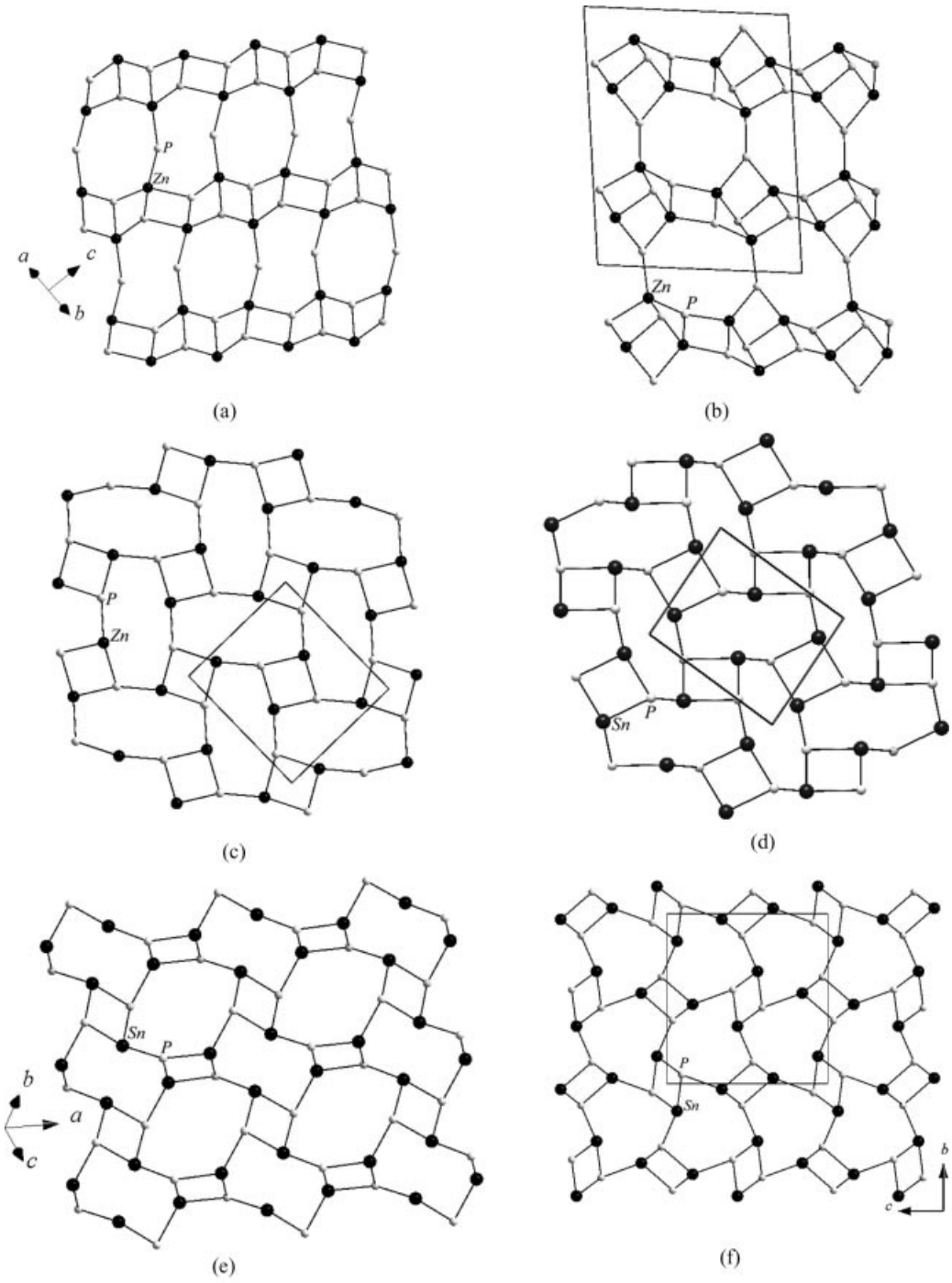

Figure 8. (a) View of the T-atom (T = Zn, P) connectivity within the layer in the zinc phosphite $[C_2N_2H_{10}][Zn_2(HPO_3)_3]$.[23] (b) View of the T-atom (T = Zn, P) connectivity within the layer in the zinc phosphite $[(C_4N_2H_{12})(C_5NH_4)]_4[Zn_6(HPO_3)_8]$.[24] (c) View of the T-atom (T = Zn, P) connectivity within the layer in the zinc phosphite $[C_3NH_{10}]_2[Zn_3(HPO_3)_4]$.[24] (d) T- atom (T = Sn, P) connectivity in **I** within the layer. Note the close similarity with the zinc phosphite structure (c). (e) T-atom (T = Sn, P) connectivity in **II** within the layer. (f) T-atom (T = Sn, P) connectivity in **III** within the layer.

Experimental Section

NMR Spectroscopy: Solid-state NMR experiments were carried out with a Bruker DSX 300 spectrometer operating at 7 T with a resonance frequency of 121 MHz for ^{31}P. A Bruker 5 mm double resonance probe was used for the experiments. The ^{31}P MAS spectra were recorded using standard cross-polarisation (CP) procedures and high proton decoupling employing a magic angle spinning (MAS) frequency of 7 kHz. In a typical experiment, radio-frequency fields of 120 kHz were used. The chemical shifts are reported relative to 85% H_3PO_4 as an external standard.

Synthesis: Compounds **I**–**III** were synthesised by hydrothermal methods starting from a tin phosphate gel and employing *N*,*N*′-bis(3-aminopropyl)ethylenediamine (BAPEN; for **I**) and homopiperazine (H-PIP; for **II** and **III**) as the structure-directing agents, respectively. For the synthesis of compound **I**, Sn^{II} oxalate was used as the source of tin, whereas $SnCl_2{\cdot}2H_2O$ was employed for **II** and **III**. In a typical synthesis for **I**, tin(II) oxalate (0.211 g) was dispersed in distilled water (1 mL). To this were added 85% aq. H_3PO_4 (0.07 mL) and BAPEN (0.19 mL) and the mixture was stirred at room temperature until homogeneous (ca. 30 min.). The final reaction mixture with the composition $1.0SnC_2O_4/1.0H_3PO_4/1.0BAPEN/55H_2O$ was heated in a 23 mL PTFE-lined stainless steel autoclave at 180 °C for 72 h. The initial pH of the mixture was 9.0 and there was no appreciable change in pH after the reaction. The resultant product contained large quantities of block-shaped colourless crystals along with a small quantity of white powder. The yield of the product was ca. 70% based on the metal source. For **II**, a reaction mixture with the composition $1.0SnCl_2{\cdot}2H_2O/1.0H_3PO_4/3.0(H\text{-}PIP)/55H_2O$ was heated in a 23 mL PTFE-lined stainless steel autoclave at 150 °C for 48 h. The initial pH of the mixture was 7.0 and there was no change in pH during the reaction. The product contained predominantly unidentified powder with a few isolated plate-like single crystals. The white powder product was found to be poorly crystalline and did not correspond to the structure of **II**. In spite of our repeated attempts, we were not able to prepare **II** in pure form and hence other than the single-crystal structure, we have not been able to characterise the compound completely. For **III**, a reaction mixture with the composition $1.0SnCl_2{\cdot}2H_2O/1.0H_3PO_4/3.0(H\text{-}PIP)/110H_2O$ was heated at 150 °C for 24 h resulting in large quantities of block-like single crystals (yield 60%). In all the preparations, the products were washed with deionised water and dried under ambient conditions.

Single-Crystal Structure Determinations: A suitable colourless single crystal of each compound was carefully selected under a polarising microscope and glued to a thin glass fibre. The single-crystal diffraction data were collected with a Bruker AXS Smart Apex CCD diffractometer at room temperature (293 K). The X-ray generator was operated at 50 kV and 35 mA using Mo-K_α (λ = 0.71073 Å) radiation. Data were collected with ω-scans of width 0.3°. A total of 606 frames were collected in three different settings of φ (0, 90 and 180°), keeping the sample-to-detector distance fixed at 6 cm and the detector position fixed at –25°. Pertinent experimental details of the structure determinations are listed in Table 5. The data were reduced using SAINTPLUS[25] and an empirical absorption correction was applied using the SADABS program.[26] The crystal structures were solved and refined by direct methods using SHELXL-97 present in the WinGX suite of programs.[27] The hydrogen atoms were placed in geometrically idealised positions and refined using the riding model. The last cycles in the refinements included all the atomic positions, anisotropic thermal parameters for all the non-hydrogen atoms and isotropic thermal parameters for all the hydrogen atoms. Full-matrix least-squares structure refinement against $|F|^2$ was carried out using the WinGX suite of programs.[27] CCDC-299664, -299665 and -602825 contain the supplementary crystallographic data for this paper. These data can be obtained free of charge from The Cambridge Crystallographic Data Centre via www.ccdc.cam.ac.uk/data_request/cif.

Initial Characterisations: The initial characterisations of **I** and **III** were carried out using elemental analysis, powder X-ray diffraction (XRD), thermogravimetric analysis (TGA) and infrared spectroscopy (IR). Elemental analyses of the crystals were carried out using atomic absorption spectroscopy (ThermoFinnigan FLASH EA 1112 CHNS analyser). TGA measurements were performed in an atmosphere of flowing oxygen (flow rate 50 mL min^{-1}) in the temperature range 30–800 °C (heating rate 5 °C min^{-1}). Infrared spectra were recorded in the range 400–4000 cm^{-1} using KBr pellets (Perkin-Elmer SPECTRUM 1000 instrument). The powder X-ray diffraction patterns were recorded on crushed single crystals in the 2θ range 5–50° using Cu-K_α radiation (Philips X'pert Pro). The C,

Table 5. Crystal data and structure refinement parameters for $[NH_3(CH_2)_3NH_2(CH_2)_2NH_2(CH_2)_3NH_3]{\cdot}2[Sn_2P_2O_8]$ (**I**), $[(N_2C_5H_{14})_2][Sn_4P_4O_{16}]{\cdot}3H_2O$ (**II**) and $[(N_2C_5H_{14})][Sn_2P_2O_8]{\cdot}H_2O$ (**III**).

	I	**II**	**III**
Empirical formula	$C_8H_{26}N_4O_{16}P_4Sn_4$	$C_{10}H_{32}N_4O_{19}P_4Sn_4$	$C_5H_{14}N_2O_9P_2Sn_2$
Formula mass	1033.04	1111.04	545.50
Crystal system	triclinic	triclinic	monoclinic
Space group	$P\bar{1}$ (no.2)	$P\bar{1}$ (no. 2)	$P2_1/n$ (no. 14)
a [Å]	8.010(1)	10.065(3)	8.956(2)
b [Å]	9.449(1)	11.677(3)	12.997(2)
c [Å]	9.742(1)	14.404(4)	12.911(2)
α [°]	68.54(1)	76.438(4)	90
β [°]	85.65(1)	73.189(4)	107.187(3)
γ [°]	71.88(1)	71.766(4)	90
Volume [Å^3]	651.51(2)	1519.7(7)	1435.8(4)
Z	2	2	4
$\rho_{calcd.}$ [g cm^{-3}]	2.633	2.428	2.524
λ (Mo-K_α) [Å]	0.71073	0.71073	0.71073
μ [mm^{-1}]	4.111	3.542	3.744
θ range [°]	2.25–28.00	1.50–24.71	2.28–28.03
Total data collected	7527	13678	12260
Unique data	3021	5116	3362
Observed data [$I > 2\sigma(I)$]	2889	3985	3046
Refinement method	full-matrix least squares on $\|F\|^2$	full-matrix least squares on $\|F\|^2$	full-matrix least squares on $\|F\|^2$
R indices [$I > 2\sigma(I)$]	R_1 = 0.0177,[a] wR_2 = 0.0456[b]	R_1 = 0.0352,[a] wR_2 = 0.0916[b]	R_1 = 0.0278,[a] wR_2 = 0.0618[b]
R indices (all data)	R_1 = 0.0177,[a] wR_2 = 0.0456[b]	R_1 = 0.0491,[a] wR_2 = 0.0990[b]	R_1 = 0.0324,[a] wR_2 = 0.0639[b]
Largest difference peak/hole [e Å^{-3}]	0.508/–0.706	1.191/–1.217	0.928/–0.749

[a] $R_1 = \Sigma||F_o| - |F_c||/\Sigma|F_o|$. [b] $wR_2 = \{\Sigma[w(F_o^2 - F_c^2)^2]/\Sigma[w(F_o^2)^2]\}^{1/2}$. $w = 1/[\sigma^2(F_o)^2 + (aP)^2 + bP]$, $P = [\max.(F_o^2,0) + 2(F_c)^2]/3$, where a = 0.0225 and b = 0.2629 for **I**; a = 0.0517 and b = 2.3068 for **II** and a = 0.0181 and b = 3.1629 for **III**.

H and N analyses of **I** and **III** are as follows: **I**: calcd. C 9.29, H 2.52, N 5.42; found C 9.92, H 2.64, N 5.49; **III**: calcd. C 10.97, H 2.92, N 5.12; found C 11.36, H 3.14, N 5.18. The powder X-ray diffraction patterns (XRD) for **I** and **III** indicated that the patterns were new and being entirely consistent with those simulated from the single-crystal structures.[28] The XRD pattern of the powder sample, obtained along with **I**, also indicated that it belongs to the structure of **I**. The IR spectra of **I** and **III** show similar features and the following bands were observed: **I**: $\tilde{\nu}$ = 3000 [ν_s(N–H)], 2824 [ν_s(C–H)], 1602 [δ(N–H)], 1465 [δ(C–H)], 1406 [ν_s(C–N)], 1334 [ν_s(C–C)], 1153 [$\nu_{as}(PO_4)$], 755 [$\nu_s(PO_4)$], 625 [δas(PO_4)], 583 [δs(PO_4)] cm^{-1}; **III**: $\tilde{\nu}$ = 3554 [ν_s(O–H)], 3099 [ν_s(N–H)], 2804 [ν_s(C–H)], 1619 [δ(O–H)], 1505 [δ(N–H)], 1431 [δ(C–H)], 1377 [ν_s(C–N)], 1238 [ν_s(C–C)], 1109 [$\nu_{as}(PO_4)$], 843 [$\nu_s(PO_4)$], 638 [δas(PO_4)], 587 [δs(PO_4)] cm^{-1}. The TGA studies on **I** were carried out in flowing air (50 mL min^{-1}) in the temperature range 25–800 °C (heating rate 10 °C min^{-1}). The results indicate one sharp weight loss in the at around 325 °C with a tail up to 475 °C followed by a small increase in the weight. The observed weight loss of ca. 15% in the range 325–500 °C corresponds to the loss of the amine molecule (calcd. 17.2%). The weight gain of 3% after 500 °C is probably the result of the oxidation of Sn^{II} to Sn^{IV} in the oxygen atmosphere (calcd. 3.74%). The TGA studies of **III** showed an initial weight loss followed by a prominent one. The initial continuous weight loss of 4.14% in the temperature range 30–200 °C corresponds to the loss of the lattice water and some adsorbed water (calcd. 3.30%). The second and more prominent weight loss of 15.5% in the range 300–700 °C corresponds to the loss of the amine molecule (calcd. 18.6%). Similar to **I**, beyond 700 °C there was a small weight gain of 2.75% which may be due to the oxidation of Sn^{II} to Sn^{IV} in the oxygen atmosphere. In both cases, the powder X-ray diffraction pattern of the decomposed samples indicated a poorly crystalline $Sn^{IV}P_2O_7$ phase (JCPDS: 29-1352). It seems likely that an amorphous phase with a ratio Sn/P > 1:1 is also present.

Supporting Information (for details see the footnote on the first page of this article): Asymmetric units for all the compounds (**I**–**III**), experimental and simulated powder XRD patterns, IR spectra and TGA curves for compounds **I** and **III**.

Acknowledgments

S. N. thanks the Department of Science and Technology (DST), Government of India for the award of a research grant. The authors also thank DST-IRPHA for the BRUKER-CCD facility.

[1] A. K. Cheetham, T. Loiseau, G. Ferey, *Angew. Chem. Int. Ed.* **1999**, *38*, 3268–3292.
[2] C. N. R. Rao, S. Natarajan, A. Choudhury, S. Neeraj, A. A. Ayi, *Acc. Chem. Res.* **2001**, *34*, 80–87.
[3] S. Ayyappan, A. K. Cheetham, S. Natarajan, C. N. R. Rao, *J. Solid State Chem.* **1998**, *139*, 207–210.
[4] S. Natarajan, *J. Mater. Chem.* **1998**, *8*, 2757–2760.
[5] S. Ayyappan, X. Bu, A. K. Cheetham, S. Natarajan, C. N. R. Rao, *Chem. Commun.* **1998**, 2181–2182.
[6] S. Natarajan, A. K. Cheetham, *J. Solid State Chem.* **1998**, *140*, 435–439.
[7] R. Vaidhyanathan, S. Natarajan, *J. Mater. Chem.* **1999**, *9*, 1807–1811.
[8] Y.-L. Liu, G.-S. Zhu, J.-S. Chen, L.-Y. Na, J. Hua, W.-Q. Pang, R.-R. Xu, *Inorg. Chem.* **2000**, *39*, 1820–1822.
[9] S. Natarajan, M. P. Attfield, A. K. Cheetham, *Angew. Chem. Int. Ed. Engl.* **1997**, *36*, 978–980.
[10] S. Natarajan, A. K. Cheetham, *Chem. Commun.* **1997**, 1089–1090.
[11] S. Natarajan, S. Ayyappan, A. K. Cheetham, C. N. R. Rao, *Chem. Mater.* **1998**, *10*, 1627–1631.
[12] S. Natarajan, M. Eswaramoorthy, A. K. Cheetham, C. N. R. Rao, *Chem. Commun.* **1998**, 1561–1562.
[13] S. Natarajan, *J. Solid State Chem.* **1999**, *148*, 50–55.
[14] G. H. Bonavia, R. C. Haushalter, S. Lu, C. J. O'Conner, J. Zubieta, *J. Solid State Chem.* **1997**, *132*, 144–150.
[15] P. J. Zapf, D. J. Rose, R. C. Haushalter, J. Zubieta, *J. Solid State Chem.* **1996**, *125*, 182; P. J. Zapf, D. J. Rose, R. C. Haushalter, J. Zubieta, *J. Solid State Chem.* **1997**, *132*, 438–442.
[16] B. Adair, S. Natarajan, A. K. Cheetham, *J. Mater. Chem.* **1998**, *8*, 1477–1479.
[17] B. Dickens, E. Prince, L. W. Schroeder, T. H. Jordan, *Acta Crystallogr. Acta Crystallogr. Sect. B* **1974**, *30*, 1470–1473.
[18] S. Natarajan, L. van Wullen, W. Klein, M. Jansen, *Inorg. Chem.* **2003**, *42*, 6265–6273.
[19] W. T. A. Harrison, Z. Bircsak, L. Hanooman, Z. Zhang, *J. Solid State Chem.* **1998**, *136*, 93–102.
[20] A. M. Chippindale, C. Turner, *J. Solid State Chem.* **1997**, *128*, 318–322.
[21] S. Natarajan, *J. Mater. Chem.* **1998**, *8*, 2757–2760.
[22] R. H. Jones, A. M. Chippindale, S. Natarajan, J. M. Thomas, *J. Chem. Soc., Chem. Commun.* **1994**, 565–566.
[23] Z. E. Lin, J. Zhang, S. T. Zheng, G. Y. Yang, *Solid State Sci.* **2004**, *6*, 371–376.
[24] S. Mandal, S. Natarajan, *Solid State Sci.* **2006**, *8*, 388–396.
[25] SMART (v. 5.628), SAINT (v. 6.45a), XPREP and SADABS, Bruker AXS Inc. Madison, Wisconsin, USA, **2004**.
[26] G. M. Sheldrick, *SADABS, Siemens Area Detector Absorption Correction Program*, University of Göttingen, Göttingen, Germany, **1994**.
[27] WinGX (v. 1.64.05), Crystallograhic Program for Windows, **2003**.
[28] W. Krauss, G. Notze, *Powder Cell for Windows*, v. 2.4, Federal Institute for Materials Research and Testing, Berlin, Germany, **2000**.

Received: March 28, 2006
Published Online: July 11, 2006

